

Optimal Heartbeat Energy Harvesting using Electrostatic Energy Harvesters

Meisam Pourahmadi-Nakhli, Bahareh Sasanpour, Mostafa Mahdavi,*
and Mohsen Sharifpur*

Microelectromechanical system of electrostatic energy harvesters is modeled using a nonlinear state–space approach in this research. The analytical models of in-plane overlap, in-plane gap closing, and their compound structures are used to analyze the energy harvesting performance from heartbeats-generated vibrations. The detailed models of both electrical and mechanical subsystems including stopper function, motion drag, parasitic capacitors, and energy converter capacitors are developed in the format of state–space equations. To reach the optimal heartbeat energy harvesting, typical 1D harvesters are developed and allowed to move in x – y and x – y – z directions. Accordingly, the optimal harvester combines the features of in-plane overlap and in-plane gap closing energy conversions, and so allows efficient absorption of energy released by heartbeat in different directions. This 3D feature gives a considerable rise to power generation to 35.038 μw at the same size compared to the new rate of the in-plane overlap or in-plane gap-closing electrostatic harvesters individually.

harvesting (or scavenging) is an attractive technique for a wide variety of self-powered microsystems such as wireless sensors, biomedical implants, military monitoring devices, structure-embedded instrumentation, remote weather stations, calculators, watches, Bluetooth headsets, etc.^[2] Electrical power microgenerators, except for piezoelectric, commonly use electromagnetic or electrostatic fields as an interface to convert kinetic energy into an electrical form.^[3] In electromagnetic devices, the energy conversion is explained with conventional permanent magnets and coils as well as with magnetorestrictive materials.^[3] An efficient electromagnetic-based energy conversion requires a considerable volume of either magnetic materials or current carrying windings; therefore, electromagnetic-based energy conversion is commonly the case

1. Introduction

Extracting power from ambient vibrations is generally known as energy harvesting, or energy scavenging.^[1] Energy (or power)


for large-scale power generation plants not for generations in microsized. Electrostatic energy harvesting devices usually have been demonstrated using capacitor structures with moving electrodes capable of producing much denser field energy than electromagnetic generators of the same size.^[4] Due to denser energy stored in their fields among the existing field through energy converters, electrostatic transducers are more suitable and compatible for microtechnologies.^[4,5]

M. Pourahmadi-Nakhli
Department of Electrical and Computer Engineering
University of Hormozgan
Bandar Abbas 7916193145, Iran

B. Sasanpour
Independent Researcher
Fars Construction Engineering Organization
Hormozgan 7184755354, Iran

M. Mahdavi, M. Sharifpur
Department of Mechanical and Aeronautical Engineering
University of Pretoria
Pretoria 0002, South Africa
E-mail: mostafa.mahdavi@up.ac.za; mohsen.sharifpur@up.a.za

M. Sharifpur
Department of Medical Research
China Medical University Hospital
China Medical University
Taichung 404, Taiwan

 The ORCID identification number(s) for the author(s) of this article can be found under <https://doi.org/10.1002/ente.202300569>.

© 2023 The Authors. Energy Technology published by Wiley-VCH GmbH. This is an open access article under the terms of the Creative Commons Attribution License, which permits use, distribution and reproduction in any medium, provided the original work is properly cited.

DOI: 10.1002/ente.202300569

Biomedical application of energy harvesters is of critical significance in energizing implanted devices with a long-life energy supply.^[6] Using conventional batteries to feed the implanted sets is not a suitable choice, as it requires further surgeries for the replacement of the run-out battery.^[6] For example, implanted pacemakers that function autonomously require a permanent power source nearby.^[7] However, the energy harvester of this application should not influence the heart pulsation since attaching the harvester to the exterior of the heart can load the heart and impede its natural function.^[8]

There are three major structures of electrostatic energy harvesters: 1) in-plane overlap, 2) in-plane gap closing, 3) out-of-plane gap closing.^[9] Guillemet et al.^[10] investigated the generated power of the two structures of out-of-plane gap closing and in-plane gap closing to optimize in terms of mechanical and electrical parameters at the same time.

An electrostatic MEMS energy converter technology was reported by Meninger et al.^[11] including the generator, its associated control circuitry, and a low power delay lock loop (DLL) system autonomously locked to ambient vibration

frequency. The proposed scheme was anticipated to generate the total power of $8.6 \mu\text{W}$ from ambient mechanical vibration of 2520 Hz.

Despesse et al.^[12] investigated two prototypes of in-plane gap-closing electrostatic harvesters: one made of silicon in microscale ($81\text{mm}^2 \times 0.4 \text{mm}$) and the other one made of tungsten in macroscale ($18 \text{cm}^2 \times 1 \text{cm}$). The explanatory structures are subjected to scavenge the available vibrations below 100 Hz from ambient environments like vibration of drill, metallic stairs, and engine motor. The silicon-made harvester showed to have a power per size of $2.16 (\mu\text{W mm}^{-3})$ compared to maximum capability of $0.33 (\mu\text{W mm}^{-3})$ for the macrostructure.

Zhu et al.^[13] introduced a two degrees of freedom (2-DoF) moving capacitor mass of $1000 \times 1000 \times 25 (\mu\text{m}^3)$ to scavenge the ultrasonic energy within two resonant frequencies of 39.238 kHz and 39.266 kHz from vibrations in the x - y plane. The harvested energy from ambient ultrasound was identified 0.1 nW through $1 \text{M}\Omega$ load resistance. Fowler et al.^[14] presented a new MEMS ultrasonic energy harvester as an extension of the research conducted by Zhu et al.,^[13] with the ability to move in the x - y - z coordinate, and the added ability of movement along Z direction that could raise the harvested energy to 12.6 nW in similar condition. Although electromagnetic energy conversion is widely used in large-scale generators, Li et al.^[15] and Peng et al.^[16] presented high-performance small-scale harvesting schemes based on abrupt magnetic flux density. Performances of electromagnetic harvesters based on alternating polarity are also investigated by Li et al.^[17]

Tvedt et al.^[18] simulated a high-pass in-plane overlap structure using PSPICE software and they concluded that maximum power of 37.05 nW was harvested through its moving mass with an acceleration amplitude of 1 g, frequency of 1190 Hz, and load resistance of $28 \text{M}\Omega$. It is often challenging to translate complex nonlinear electromechanical systems to linear electrical elements solved by SPICE.^[18] To overcome this issue and analyze heartbeat energy harvesting, herein a detailed model of electromechanical system including parasitic capacitors, motion drags, and limiting steppers are developed in the form of nonlinear state-space equations. Contrary to the PSPICE platform used by Tvedt et al.,^[18] the state-space approach of this work provides good flexibility in modeling and simulation of the harvester performance under different system variation of inputs and parameters. The harvester exposed to heartbeat excitation in interventricular septum as an efficient place for energy harvesting is simulated through a numerical state-space modeling. The generated power is evaluated under different scenarios of pre-charge voltage inputs and loading conditions.

2. Methodology

In this research, we aim to extend the scheme proposed by Tvedt et al.^[18] and Truong et al.^[19] to harvest the energy of the heartbeat acceleration spectrum principally less than 100 Hz. The methodology of this research which is based on analytic modeling of the harvester and simulation of exposure to heartbeat acceleration is as follows: 1) Taking the in-plane overlap structure with only able to move and so extract the acceleration along x direction. 2) Initiating dimensions, parameters of drags, steppers, and

springs to set the harvester for heartbeat frequencies. 3) Developing the model by allowing the movement of the mass along one, two, and three dimensions; Developing the state-space equations of the electric and mechanical subsystems with expanded freedom of movement. 4) Simulation of the exposure of the harvester to measured interventricular accelerations. 5) Time domain numerical solution of discretized state-space equations.

3. Electromechanical Energy Conversion in Electrostatic Transducers

Electrical and magnetic fields as a boundary between electrical and mechanical systems account for the interface in energy conversion between them. In fact, the fields are able to store the electrical and mechanical powers within and release the stored energy in terms of work through displacements. For electrostatic energy stored in a capacitor, the displacement produces the instantaneous force in Newton as

$$F_T = \frac{q_i^2}{2} \frac{d}{dx} \left(\frac{1}{C_i(x)} \right) \quad (1)$$

where q_i is the electric charge on variable capacitors, C_i is the capacitance of variable capacitors, and i is the number of capacitors. Variable x is the displacement of the proof mass (m).

Equation (1) establishes an important relationship between electrical and mechanical systems in an electrostatic energy harvester. To gain a basic perception of the modeling approach for various harvesters in this study, it is useful to consider the

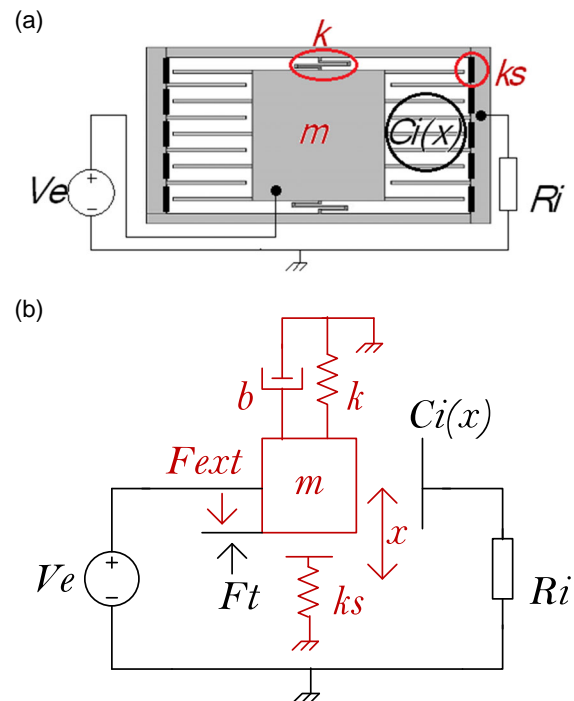


Figure 1. a) 1D electrostatic comb electrodes scheme of capacitor $C_i(x)$, b) The primary model of the electrostatic transducer. Electrical (in black) and mechanical (in red).

electrostatic transducer of **Figure 1**. The electric charges on capacitor plates are flashed initially by electret voltage V_e due to Fermi energy voltage connected. This initial voltage produces the electric field between plates and corresponding charges on plates. Basically, the capacitance between plates changes as a result of displacements and if the voltage is assumed constant, it means the change of charge; a current triggered by displacement. Just as in electromagnetic energy conversion, magnetic energy changes due to displacement in a winding produce or absorb mechanical energy, in electrostatic energy conversion electric field energy variations due to displacements in a capacitor produce or absorb mechanical energy. The electric energy in electromagnetic conversion originates in an alternating form voltage, while the same electric energy is produced in an alternating current in electrostatic conversion.^[18]

$$V_{Li} = V_e + \frac{q_i}{C_i(x)} \quad (2)$$

$$\dot{q}_i = -\frac{V_{Li}}{R_{Li}} = -\frac{V_e}{R_{Li}} - \frac{q_i}{R_{Li}C_i(x)} \quad (3)$$

For the mechanical subsystem, by applying the motion equation along the x direction it follows

$$m\dot{v}_m = F_{ext} - b\dot{x} - kx - F_T - f_s \quad (4)$$

$$\dot{x} = v_m \quad (5)$$

For a mass (m) exposed to an external accelerating movement, one can identify the force as $F_{ext} = ma$.

The structure includes stoppers to limit the mass displacement to prevent the electrode's electrical connection (short circuit) as well as mechanical damage. The function of the elastic stoppers is modeled by stiff springs (k_s) that operate only when displacements are larger than x_s (see **Figure 2**).

Stoppers-driven force is

$$F_s = \begin{cases} 0 & -x_s \leq x \leq x_s \\ -k_s(x + x_s) & x < -x_s \\ -k_s(x - x_s) & x > x_s \end{cases} \quad (6)$$

Finally, the basic system's equation can be written in terms of variables $X = [q_i \ v_m \ x]^T$ and inputs $U = [F_{ext} \ V_e]^T$

$$\dot{X} = \begin{bmatrix} -\frac{1}{R_{Li}C_i(x)} & 0 & 0 \\ -\frac{q_i}{2m} \frac{d}{dx} \left(\frac{1}{C_i(x)} \right) & -\frac{b}{m} & -\frac{k}{m} - \frac{k_s(x)}{m} \\ 0 & 1 & 0 \end{bmatrix} X + \begin{bmatrix} 0 & -\frac{1}{R_{Li}} \\ \frac{1}{m} & 0 \\ 0 & 0 \end{bmatrix} U \quad (7)$$

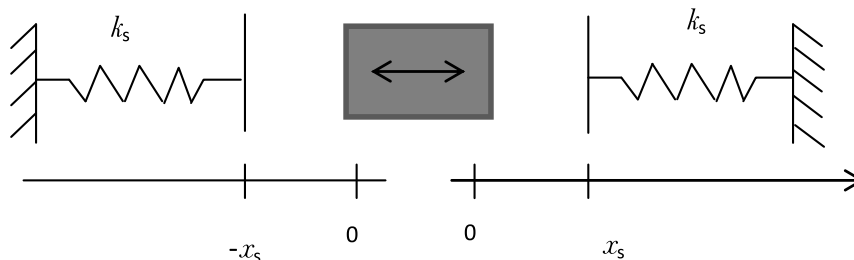


Figure 2. Stoppers function in displacements larger than x_s .

$$\dot{X} = f(X, U) \quad (8)$$

Equation (1)–(8) can be generalized to other models for displacements in directions (y) , (x,y) , and (x,y,z) and $i = 1, \dots, 4$.

4. Models with One Degree of Freedom in Displacement

4.1. In-Plane Overlap Electrostatic Energy Harvester

The mechanical energy in this structure is converted into the electrical form through derivation of the stored electrical field energy with respect to change in capacitor's electrode overlap. **Figure 3** and **4**, respectively, show the capacitor structure and the equivalent circuit of the in-plane overlap electrostatic harvester.

The major challenge seems to be how to bias electrostatic harvesters. The harvester needs to be flashed at the beginning of its operation. A design that employs an electret as an internal bias and therefore avoids the need for external bias is considered for the current article. The precharge voltage here generated by electrets is V_e . C_1 and C_2 are variable capacitors, and C_p is a parasitic capacitor between electrodes and reference points. The variable capacitors are a function of the overlap value of the electrodes

$$C_1(x) = \frac{2N_g \epsilon t_f (x_0 - x)}{g_0} \quad (9)$$

$$C_2(x) = \frac{2N_g \epsilon t_f (x_0 + x)}{g_0} \quad (10)$$

The overlap of capacitances, C_1 and C_2 , changes by the displacement of moving mass, and the counter-force is generated as

$$F_{Tx} = \frac{q_1^2}{2} \frac{d}{dx} \left(\frac{1}{C_1(x)} \right) + \frac{q_2^2}{2} \frac{d}{dx} \left(\frac{1}{C_2(x)} \right) \quad (11)$$

4.2. In-Plane Gap Closing Electrostatic Energy Harvester

In this structure, energy is converted through the gap variation between capacitor electrodes, as shown in **Figure 5** and **6**.

Because of equal displacement of both side fingers, the operation of both side capacitors can be presented by one equivalent capacitor (C_1) which changes by y displacement.

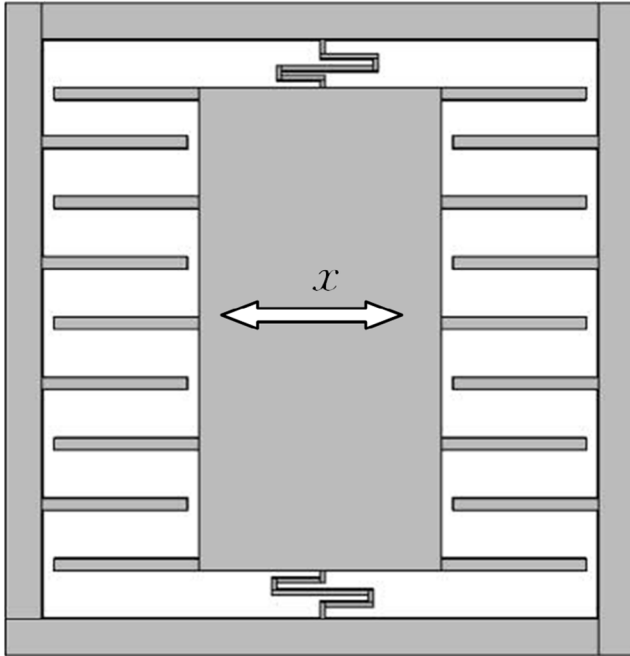


Figure 3. Capacitor structure of in-plane overlap electrostatic energy harvester.

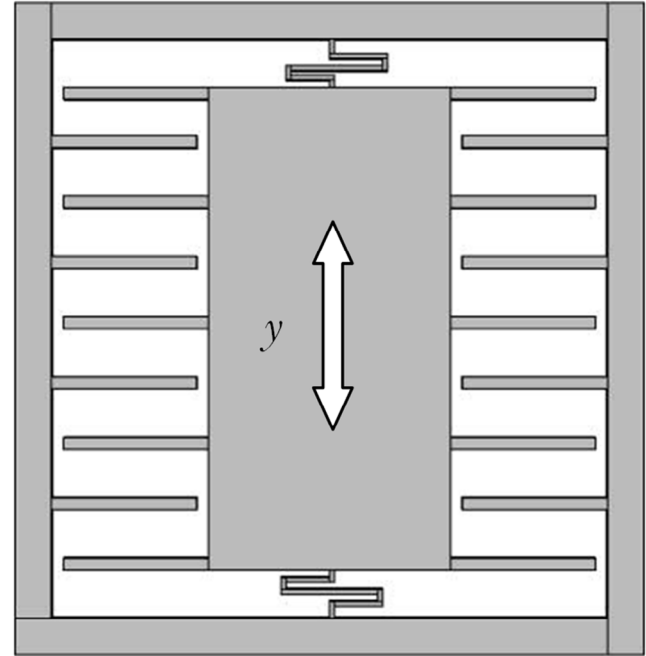


Figure 5. The capacitor structure of the in-plane gap closing electrostatic energy harvester.

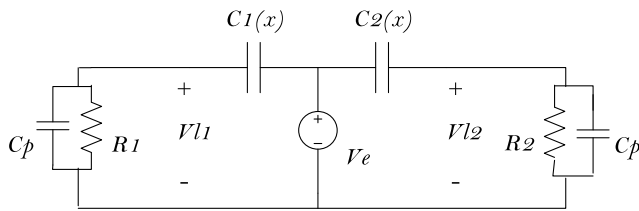


Figure 4. Electrical equivalent circuit of the in-plane overlap electrostatic energy harvester.

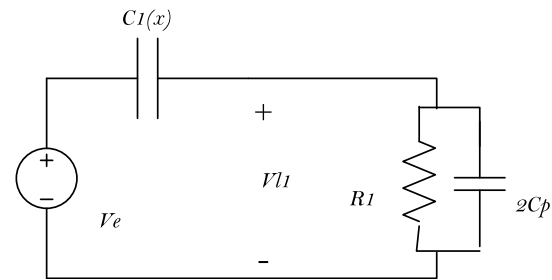


Figure 6. The electrical equivalent circuit of in-plane gap closing electrostatic energy harvester.

$$C_1(y) = \frac{2g_0 \epsilon L_f t_f N_g}{g_0^2 - y^2} \quad (12)$$

The gap between the capacitor electrodes changes by finger displacement and it results in the electromotive force

$$F_{Ty} = \frac{q_1^2}{2} \frac{d}{dy} \left(\frac{1}{C_1(y)} \right) \quad (13)$$

5. The Compound Electrostatic Energy Harvester with Two Degrees of Freedom in Movement

The compound electrostatic energy harvester with 2-DoF is shown in **Figure 7**. This structure comprises of four identical comb capacitors each of which is free to move in x and y directions.

In this structure, the capacitor electrodes are allowed to move in X - Y plane. Therefore, the variation of capacitors results in the electrical equivalent circuit of **Figure 8**. According to the x and y directions in **Figure 7**, C_1 to C_4 are in the following form

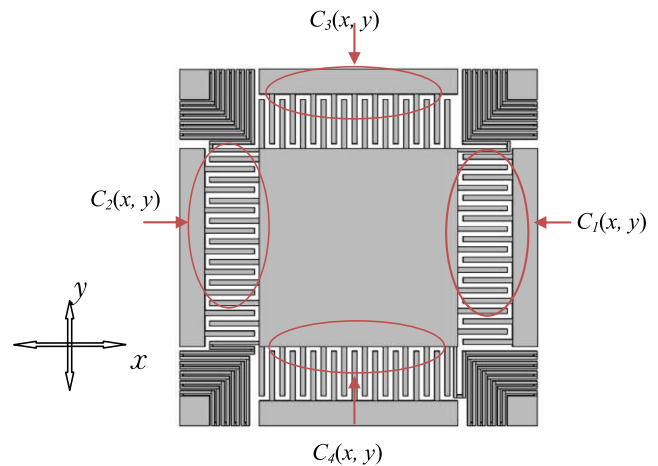


Figure 7. The capacitor structure of compound transducer with two degrees of freedom in movement.

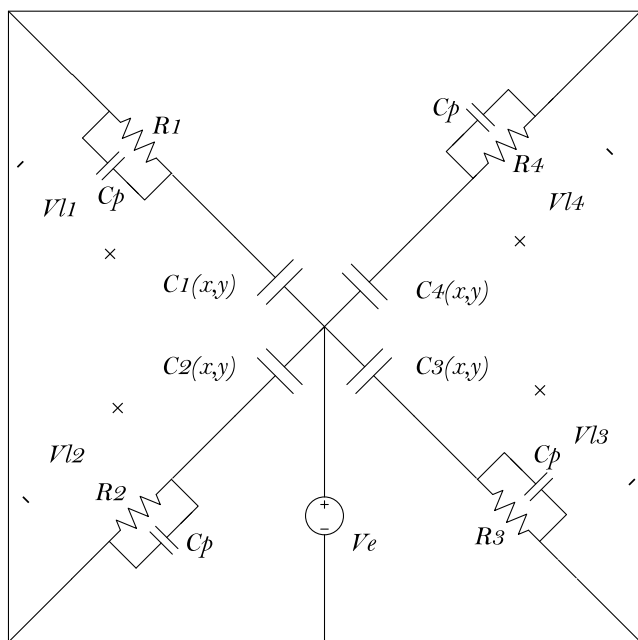


Figure 8. The electrical equivalent circuit of the compound transducer with two degrees of freedom in motion.

$$C_1(x, y) = \frac{2N_g \epsilon t (x_0 - x) y_0}{y_0^2 - y^2} \quad (14)$$

$$C_2(x, y) = \frac{2N \epsilon t (x_0 + x) y_0}{y_0^2 - y^2} \quad (15)$$

$$C_3(x, y) = \frac{2N \epsilon t (y_0 - y) x_0}{x_0^2 - x^2} \quad (16)$$

$$C_4(x, y) = \frac{2N \epsilon t (y_0 + y) x_0}{x_0^2 - x^2} \quad (17)$$

The components of electromechanical force along x and y directions driven by all capacitors can be expressed as

$$F_{Tx} = \sum_{i=1}^4 \frac{q_i^2}{2} \frac{\partial}{\partial x} \frac{1}{C_i(x, y)} \quad (18)$$

$$F_{Ty} = \sum_{i=1}^4 \frac{q_i^2}{2} \frac{\partial}{\partial y} \frac{1}{C_i(x, y)} \quad (19)$$

6. The Compound Electrostatic Energy Harvester with Three Degrees of Freedom

The capacitor structure of the 3D harvesters and their equivalent circuit is similar to the 2D one (Figure 9 and 10). However, the variable capacitor is a function of x , y , and z displacements. Therefore, an extra mechanical equation in z direction appears in the state-space equations.

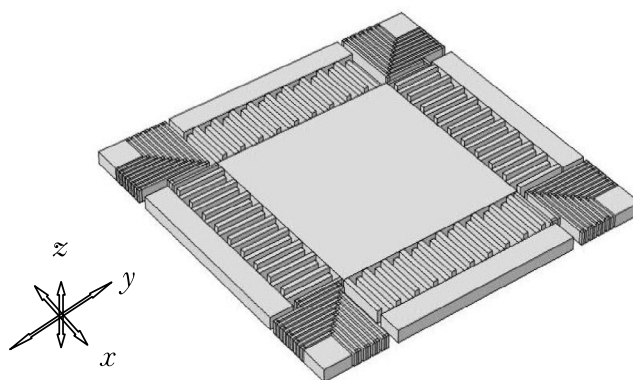


Figure 9. The capacitor structure of compound electrostatic energy harvester with three degrees of freedom in motion.

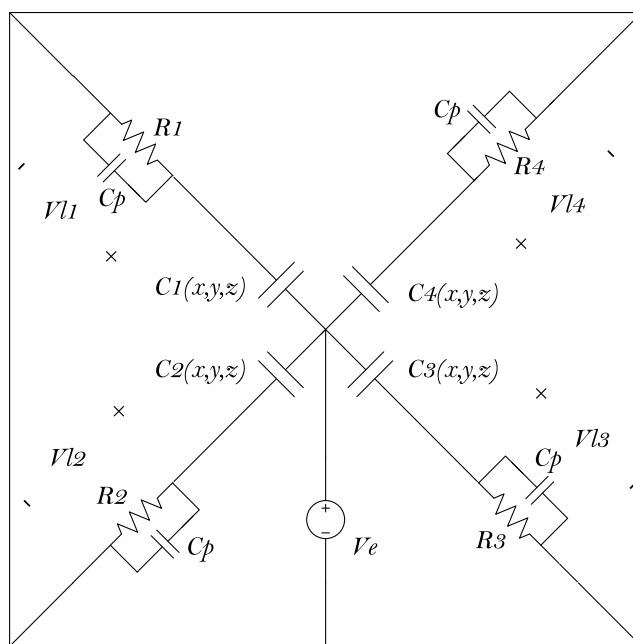


Figure 10. Electrical equivalent circuits of compound electrostatic energy harvester with three degrees of freedom.

The capacitor functions of x , y , and z variables are

$$C_1(x, y, z) = \frac{2N_g \epsilon (z_0 - z) (x_0 - x) y_0}{y_0^2 - y^2} \quad (20)$$

$$C_2(x, y, z) = \frac{2N_g \epsilon (z_0 - z) (x_0 + x) y_0}{y_0^2 - y^2} \quad (21)$$

$$C_3(x, y, z) = \frac{2N_g \epsilon (z_0 - z) (y_0 - y) x_0}{x_0^2 - x^2} \quad (22)$$

$$C_4(x, y, z) = \frac{2N_g \epsilon (z_0 - z) (y_0 + y) x_0}{x_0^2 - x^2} \quad (23)$$

$$F_{Tx} = \sum_{i=1}^4 \frac{q_i^2}{2} \frac{\partial}{\partial x} \frac{1}{C_i(x, y, z)} \quad (24)$$

Table 1. The characteristics of structures under study.

Parameters	IPO	IPGC	2D compound	3D compound
Length of fingers, L_f	100 μm	100 μm	100 μm	100 μm
Width of fingers, W_f	4 μm	4 μm	4 μm	4 μm
Thickness of capacitor fingers, t_f	100 μm	100 μm	100 μm	100 μm
Gap between capacitor fingers, g_0	3 μm	15 μm	15 μm	15 μm
Number of capacitor finger pairs, N_g	357	130	130	130
Mass, m	5.89 mg	5.85 mg	5.85 mg	5.85 mg
Spring constant, k	0.25 N m^{-1}	0.25 N m^{-1}	0.25 N m^{-1}	0.25 N m^{-1}
Damping constant, b	$8.45 \times 10^{-4} \text{ N-s m}^{-1}$	$8.45 \times 10^{-4} \text{ N-s m}^{-1}$	$8.45 \times 10^{-4} \text{ N-s m}^{-1}$	$8.45 \times 10^{-4} \text{ N-s m}^{-1}$
Electret voltage, V_e	5 v	5 v	5 v	5 v
Parasitic capacitance, C_p	1,94 pf	1,94 pf	1,94 pf	1,94 pf
Initial finger overlap, x_0	80 μm	99 μm	85 μm	85 μm
Initial finger overlap, y_0	3	15	15	15
Initial finger overlap, z_0	–	–	–	85
Displacement limit of stoppers, x_s	19.5 μm	–	14.5 μm	14.5 μm
Displacement limit of stoppers, y_s	–	14.5 μm	14.5 μm	14.5 μm
Displacement limit of stoppers, z_s	–	–	–	14.5 μm
Spring constant of stoppers, k_s	326 000 N m^{-1}	326 000 N m^{-1}	326 000 N m^{-1}	326 000 N m^{-1}
Displacement limit of variable capacitors, x_c	19 μm	–	14 μm	14 μm
Displacement limit of variable capacitors, y_c	–	14 μm	14 μm	14 μm
Displacement limit of variable capacitors, z_c	–	–	–	14 μm

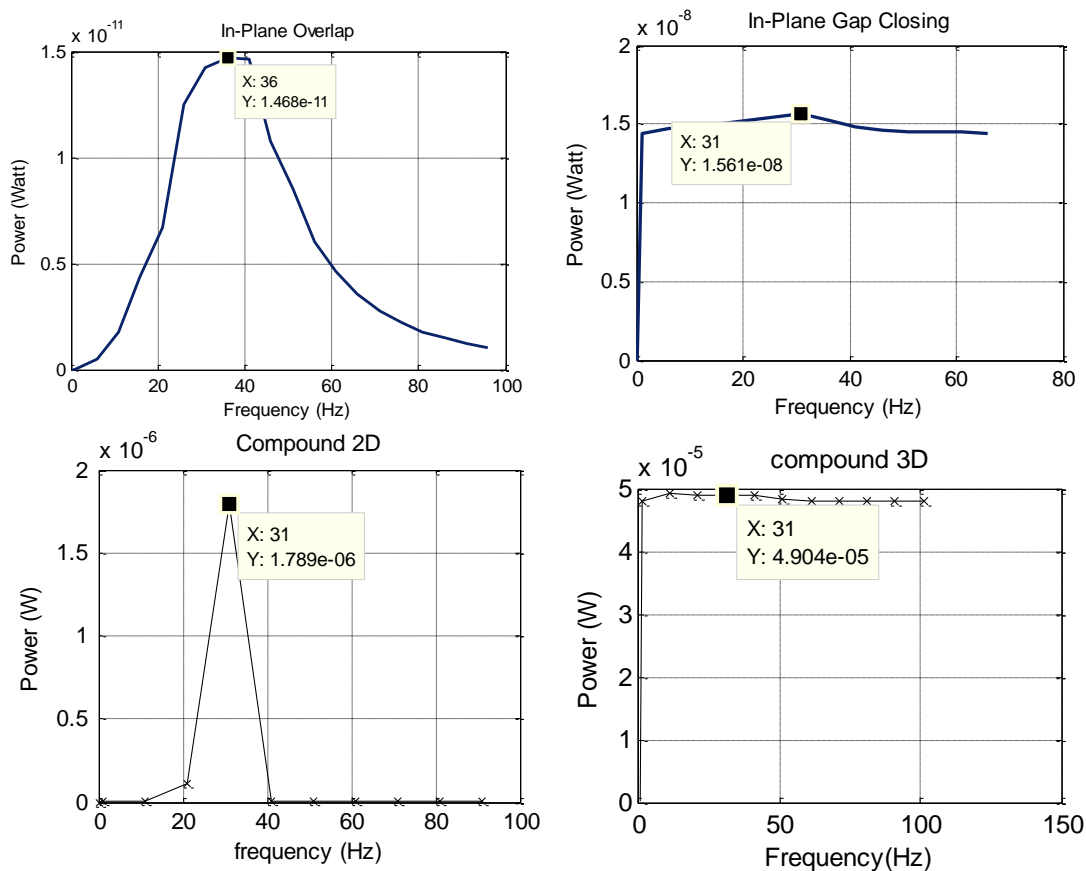


Figure 11. Power density spectrum of structure excited by $a = 0.5 \text{ m s}^{-2}$ with different frequencies.

$$F_{Ty} = \sum_{i=1}^4 \frac{q_i^2}{2} \frac{\partial}{\partial y} \frac{1}{C_i(x, y, z)} \quad (25)$$

$$F_{Tz} = \sum_{i=1}^4 \frac{q_i^2}{2} \frac{\partial}{\partial z} \frac{1}{C_i(x, y, z)} \quad (26)$$

7. Modeling and Simulation of Nonlinear State-Space Equations for Energy Harvesting from Heartbeat

Considering the following nonlinear equation

$$\dot{X} = f(X, U) \quad (27)$$

Assuming the initial condition of X_0 and U_0 , one can use the discrete form of Equation (27) as

$$\frac{X(t) - X(t - \Delta t)}{\Delta t} = f(X(t - \Delta t), U(t - \Delta t)) \quad (28)$$

For $\Delta t \rightarrow 0$ and $t > 0$ the state variables of any time t can be determined by

$$X(t) = f(X(t - \Delta t), U(t - \Delta t)) \cdot \Delta t + X(t - \Delta t) \quad (29)$$

To simulate the behavior of different types of electrostatic energy harvesters under heartbeat excitation, the typical structure of in-plane overlap harvester used by Tvedt et al.^[18] is extended to different structures of the electrostatic energy harvesters. They consist of in-plane-overlap (IPO), in-plane-gap-closing (IPGC), 2D compound, and 3D compound structures. Different parameters of the structures are presented in **Table 1**. The mechanical resonant frequency is tuned so that the harvester converts the power at frequencies less than 100 Hz. This design also makes structures suitable for harvesting the heartbeat energy content over 20 to 30 Hz. Accordingly, the spring constants of the structures are set at 0.25 N m^{-1} .

The evaluation of power spectrum characteristics is done by exciting the structure with sinusoidal acceleration of 0.5 m s^{-2} at different frequencies and load impedances. Excitation of 0.5 m s^{-2} is decomposed to have equal components along x and y for 2D harvester, and in the case of 3D harvester, the excitation is considered at 45° from z with equal components along x and y axes. **Figure 11** and **12** depict power density spectrums with different frequencies for IPGC, IPO, 2D, and 3D compound models of the electrostatic energy harvester. It is shown that maximum energy conversion under sinusoidal excitation occurs at 36 Hz (0.1468 pW), 31 Hz (15.61 nW),

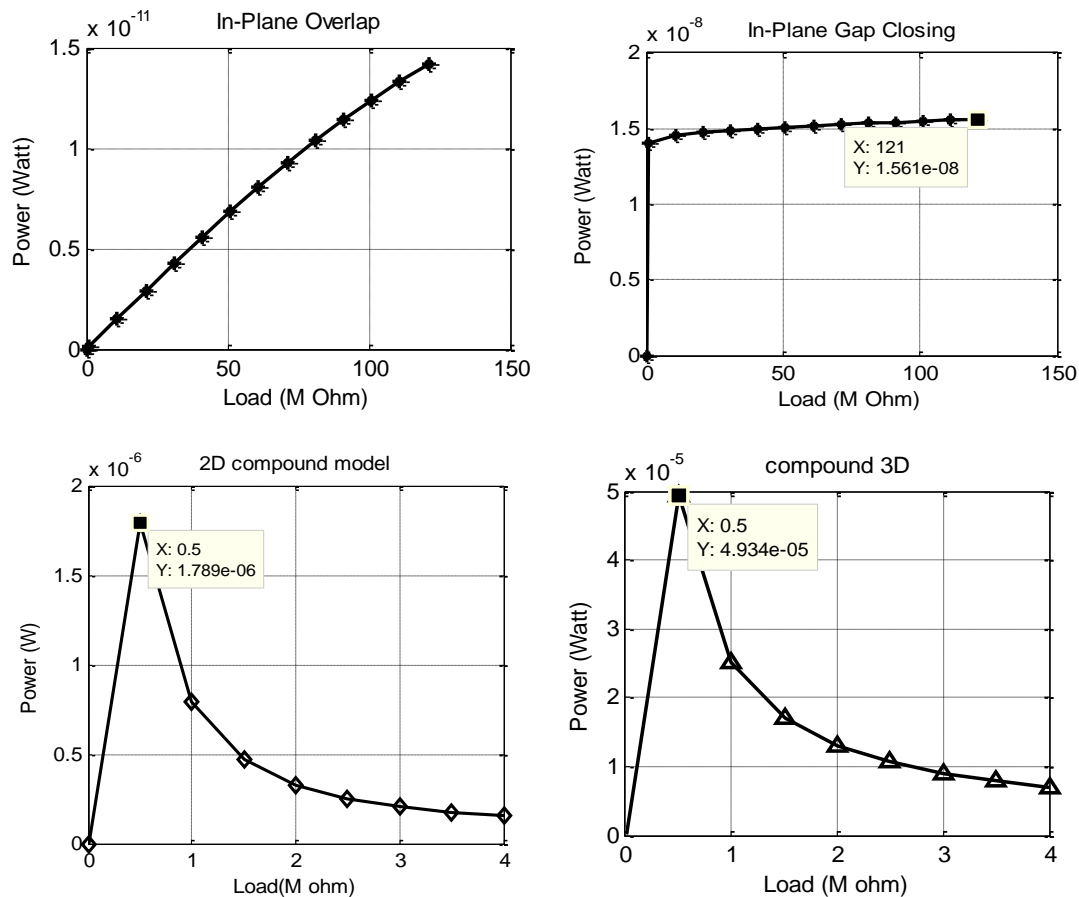


Figure 12. Power density spectrum of structures with different loads ($a = 0.5 \text{ m s}^{-2}$).

31 Hz (1.789 μ W), and 31 Hz (49.04 μ W) for IPO, IPGC, 2D, and 3D models, respectively.

For resistive loads, the N-sample periodic voltage yields the average power per cycle for all capacitors as

$$P = \sum_{i=1}^I \left(\frac{1}{N} \sum_{n=1}^N \frac{|V_{li}(n)|^2}{R_i} \right) \quad (30)$$

Figure 12 shows power density spectrums with different loads for IPGC, IPO, 2D, and 3D compound models at resonant excitation. It is shown that IPO has more energy conversion rate at higher load resistances, although the amount of energy harvested of this model is considerably lower than other models. In contrast, IPGC model has small sensitivity to the resistance change and it transforms about 15 nW power at frequency of 30 Hz. 2D and 3D structures show the same behavior due to variation of load resistances. Maximum power conversion for both 2D and 3D compound models occurs at 0.5 M Ω . However, the energy harvested of 3D model is significantly higher (about 49 μ W) that makes this model suitable for low-frequency energy harvesting applications.

7.1. Energy Harvesting from Heartbeats

The reliable powering of implantable devices in human body is one of the critical applications of energy harvesting. The possibility of energy harvesting from biomotions has become an interesting subject of research since it can eliminate the problems of traditional battery-energized implantations as well as the inevitable problems of the replacement surgery of the run-out battery. One example of these implantable devices is pacemaker in which case a permanent energy source could be achieved from heartbeat excitations, schematically shown in Figure 13. For this purpose, the recorded acceleration of inter-ventricular septum as a potential implantation point^[6] is considered to excite the harvesting module.

The frequencies of one heartbeat can be in the range of 1 Hz to 1.5 Hz and depending on the physical activities it is subject to change and may reach 3 Hz. Moreover, the fast variation of acceleration adds high-frequency content to the power spectrum. As shown in Figure 14, the majority of the energy content ranges up to 1000 Hz. However, investigation of such measured spectrum revealed that acceleration around the frequency range around 30 Hz has significant amplitudes. Accordingly, it is reasonable to consider low-pass harvester in the range 30 Hz for energy harvesting applications.

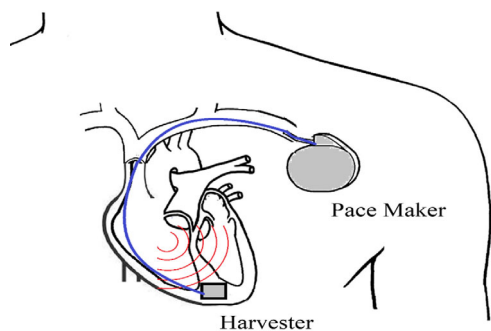


Figure 13. Harvester-Pacemaker system in a human body.

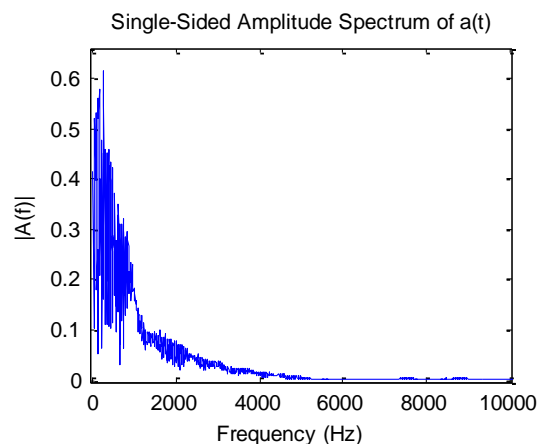


Figure 14. Power spectrum of heartbeat acceleration.

7.1.1. Energy Harvesting from Heartbeat by In-Plane Overlap Electrostatic Energy Harvester

Using model parameters of Table 1 and numerical solution of the corresponding state-space equation, the time domain displacement is calculated, as shown in Figure 15. It also indicates the displacement limit caused by stoppers located at $\pm 19 \mu$ m. Figure 16 depicts the voltage fluctuations generated by mass displacement in the electrostatic field. The relevance of voltage and displacement fluctuations can be found by comparing Figure 15 and 16. High perturbations of mass displacement especially when moving mass is repelled by stoppers have caused the voltage to gain high amplitudes. The temporary shoots in voltage waveform at 0.2, 0.5, and 0.68 s correspond to the rapid displacements at the same times. The effective voltage generated on loads and identified as the root mean square of voltage samples is 0.0148 V here. The sum power consumed by R_{11} and R_{12} is 1.7627 pW.

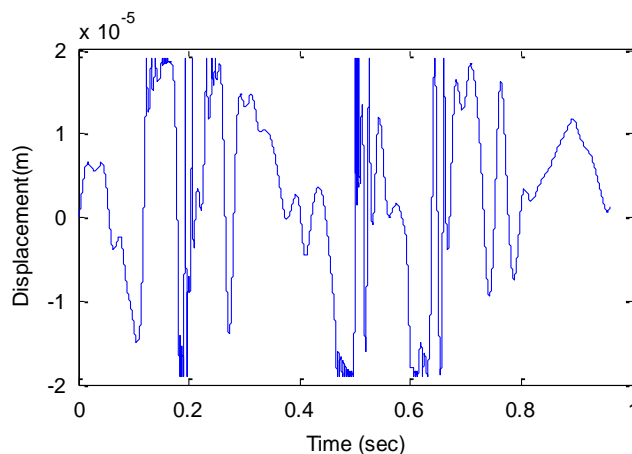


Figure 15. Displacement of moving mass in the I-P-O-e-VEHs.

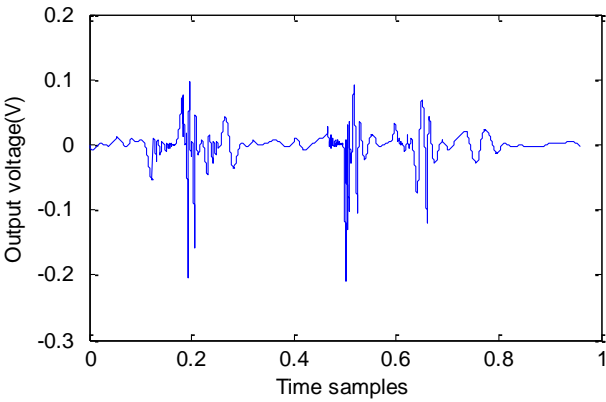


Figure 16. Voltage of the I-P-O.

7.1.2. Energy Harvesting from Heartbeat by In-Plane Gap Closing Electrostatic Energy Harvester

The in-plane gap closing electrostatic energy harvester is exposed to heartbeat excitation of Figure 13. It is assumed that the net acceleration excites the moving mass along y direction. The numerical solution of state–space yields the mass displacement and induced voltage presented in **Figure 17a,b**. The voltage of V_{12} is similar to V_{11} but with 180° of phase difference. The

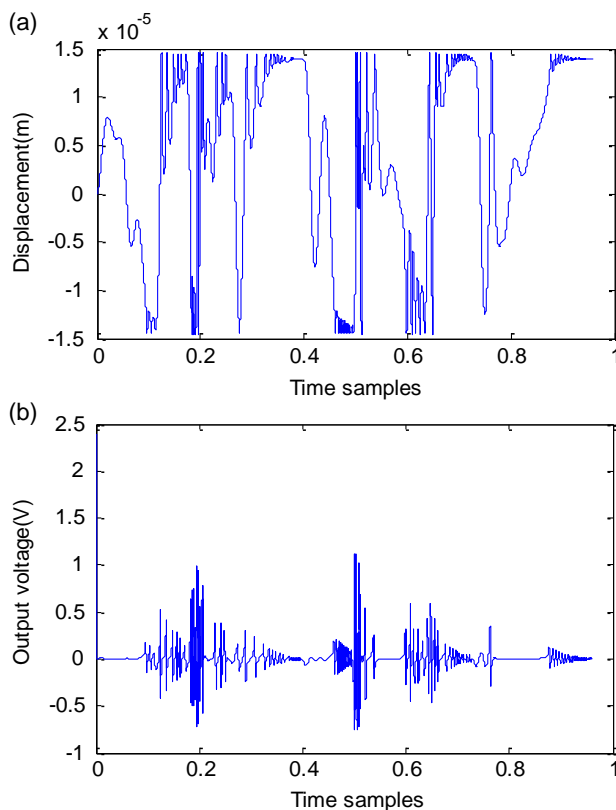


Figure 17. Displacement and induced voltage of in-plane gap closing energy harvester under heart excitation. a) y -displacement of moving mass. b) Voltage induced on R_{11} .

coincidence of temporal voltage and displacement fluctuation is more evident in Figure 17. An average power of 0.3578 nW is generated by I-P-G-C. This power value is considerably higher than the amount of power generated by in-plane overlap harvester under the same excitation. This increase in power generation is achieved as fingers of gap closing structure are at their maximum overlap leading to higher capacitive energy. Having larger energy content in the field, the gap-closing structure converts higher energy from the same mass displacement.

7.1.3. Energy Harvesting from Heartbeat by 2D Compound Electrostatic Energy Harvester

As developed in Section 4, the 2D compound model involves two independent sets of equation: one developed in x direction and the other one for the motion along y direction. Accordingly, the excitation should be introduced along two directions of x and y . To evaluate the operation of the 2D compound harvester, the external force is considered to excite the moving mass along x and y by equal decomposition of acceleration vector.

Figure 18a,b presents the time domain displacements of the moving mass along directions x and y excited by acceleration applied to previous models. Since the structure and external force are symmetric on x and y dimensions, the displacement along x direction is identical to y displacement of moving mass (compare Figure 18a,b).

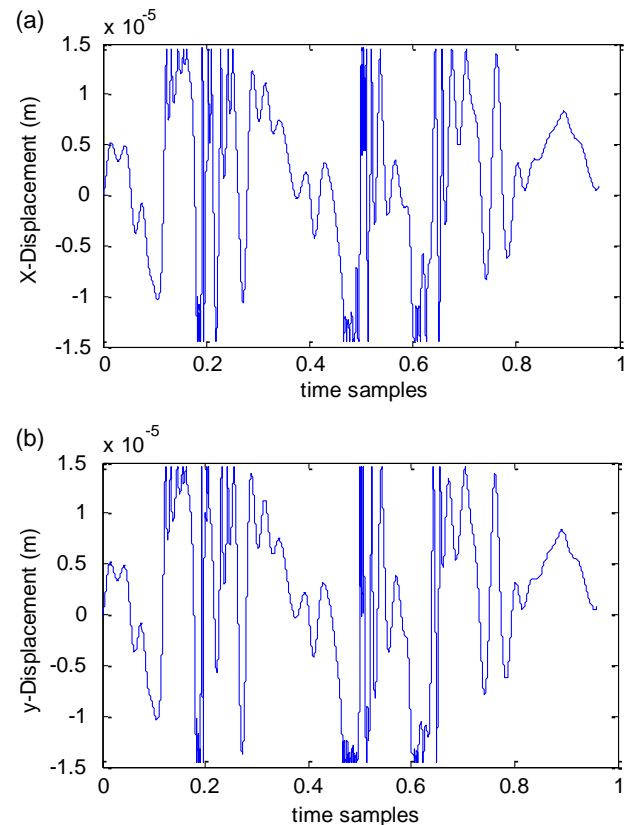


Figure 18. Displacement in x and y directions of 2D compound energy harvester. a) Displacement in x direction. b) Displacement along y direction.

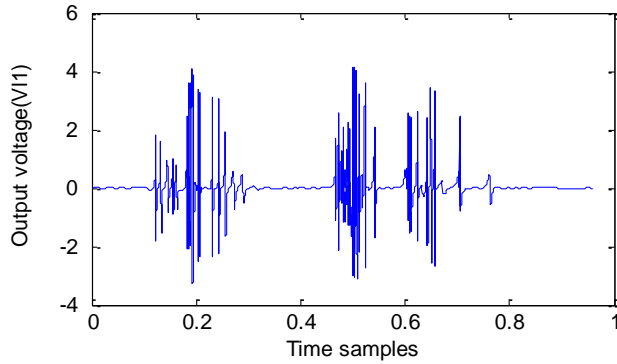


Figure 19. Wave form of voltage V_{11} and displacement x for 2D compound model under heart excitation.

Contrary to 1D models in which the voltage is generated by x or y displacement, the voltage in 2D model is induced by simultaneous x and y displacements. **Figure 19** shows the voltage on V_{11} in this condition. By comparing the total energy generation of the 2D model ($16.245 \mu\text{W}$) with 1D's (0.3578 nW), one can argue that under the same input condition by adding two combs on two sides of 1D model, the power rises up to 1000 folds.

7.1.4. Energy Harvesting from Heartbeat by 3D Compound Electrostatic Energy Harvester

In 3D compound harvester, the moving mass is allowed to move along all directions. To excite the moving mass in three dimensions, the external force in terms of acceleration is considered to have three equal components along x , y , and z axes. To achieve this, we consider moving mass is excited by the external force with direction of 45° from x , y , and z axes.

The numerical solution under this decomposed force yields the displacement waveforms of the **Figure 20a–c**. The voltage induced on each load is resulted by simultaneous displacements along x , y , and z directions (see **Figure 21**).

The power values of different harvesters excited by heartbeat are compared in **Table 2**. As shown, the generated power rises by allowing more freedom to move (along x , y , and z) so that the maximum power of $35.038 \mu\text{W}$ is harvested in case of 3D model. It is evident that by allowing the mass to move in three dimensions and decomposing same force along three axes, the 3D model is able to generate higher values than two folds compared to the 2D one. This major increase in the power (to $35.038 \mu\text{W}$) can well satisfy the energy need of the typical cardiac pacemakers demanding 30 to $100 \mu\text{W}$.^[20]

8. The Heartbeat – Energy Generation Sensitivity to Precharge Voltage

In addition to the capacitance, the electric field energy depends on the precharging voltage of the capacitor. Regardless of the technology of the precharge voltage, herein, we evaluate the impact of precharge voltage on final generation. According to **Figure 22**, the power generation of 1D (IPO) and 3D models increases as the precharge voltage increases. Although the field

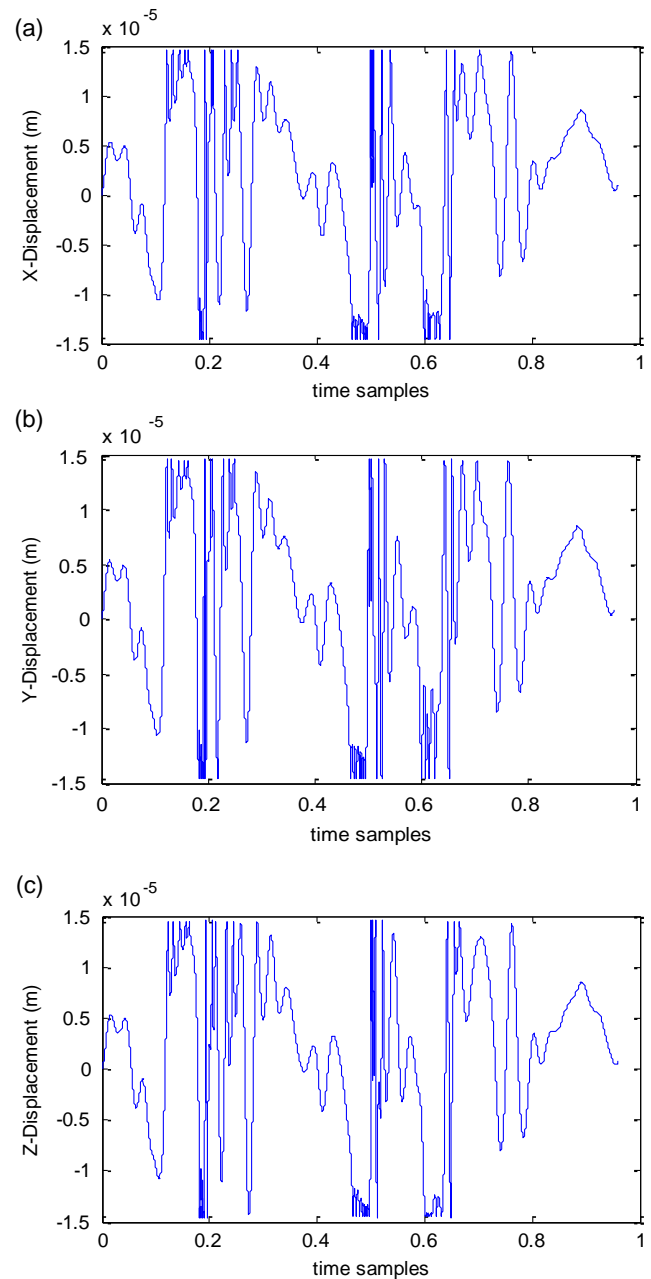


Figure 20. x , y , and z displacements of 3D compound model. a) x -displacement. b) y -displacement. c) z -displacement.

energy stored in capacitor is directly related to precharge voltage, the field energy presents a nonlinear relationship of conversion toward electrical power.

For 1D (IPGC) and 2D models, the power generation is declined for voltages higher than 8 volts due to dominant gap-closing capacitors. Following term explains why the generation in a gap-closing capacitor declines for higher voltages.

$$f_y = \frac{Ve^2}{2} \frac{\partial c(y)}{\partial y} = \frac{Ve^2}{2} \frac{\partial \left(\frac{2N_g g e L_f t_f}{g^2 - y^2} \right)}{\partial y} = \frac{Ve^2}{2} \frac{4y N_g g e L_f t_f}{(g^2 - y^2)^2} \quad (31)$$

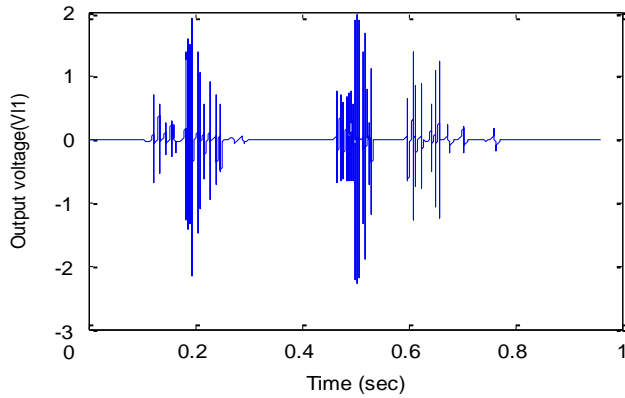


Figure 21. The generated voltage in 3D model.

Table 2. Generated power of different energy harvesters from heartbeat acceleration.

Energy harvesters	Overlap	Gap closing	Compound 2D	Compound 3D
Power	1.7627 pW	0.3578 nW	16.245 μ W	35.038 μ W
Load	100 M Ω	35 M Ω	0.5 M Ω	0.5 M Ω

The term $(g^2 - y^2)$ takes a small value when y displacement approaches to its limit. This small value in denominator and

the large value of Ve^2 in nominator of Equation (31) lead to large resisting force f_y , so that moving mass is locked at limit points (steppers). When moving mass is locked, electromechanical conversion no longer happens as a result of zero displacements.

9. The Heartbeat – Energy Generation Sensitivity to Loading Condition

For optimal energy transfer, the loads are assumed resistive. In practical implementation, the output voltage passes through an AC–DC convertor, to be able to convert the perturbed voltage to a desired DC level. A range of resistance from 0 to 100 M Ω is investigated for optimal loading. As shown in **Figure 23**, the maximum energy is converted by 3D model at the rate around 35.038 μ W to feed 0.5 M Ω load. With regard to 2D model, the maximum power of 2.1702 μ W occurs by feeding a 1 M Ω load. In spite of rising in energy conversion as resistance increases in the case of IPGC, for resistances larger than 45 M Ω , the power fluctuates around the average of 0.5 nW.

It is worth noting that the direction of excitation vector can be a contributing factor as a control variable to energy conversion. Therefore, optimizations by controlling this factor, as a guide for positioning of the implant electrostatic harvesters, can be conducted in the future researches.

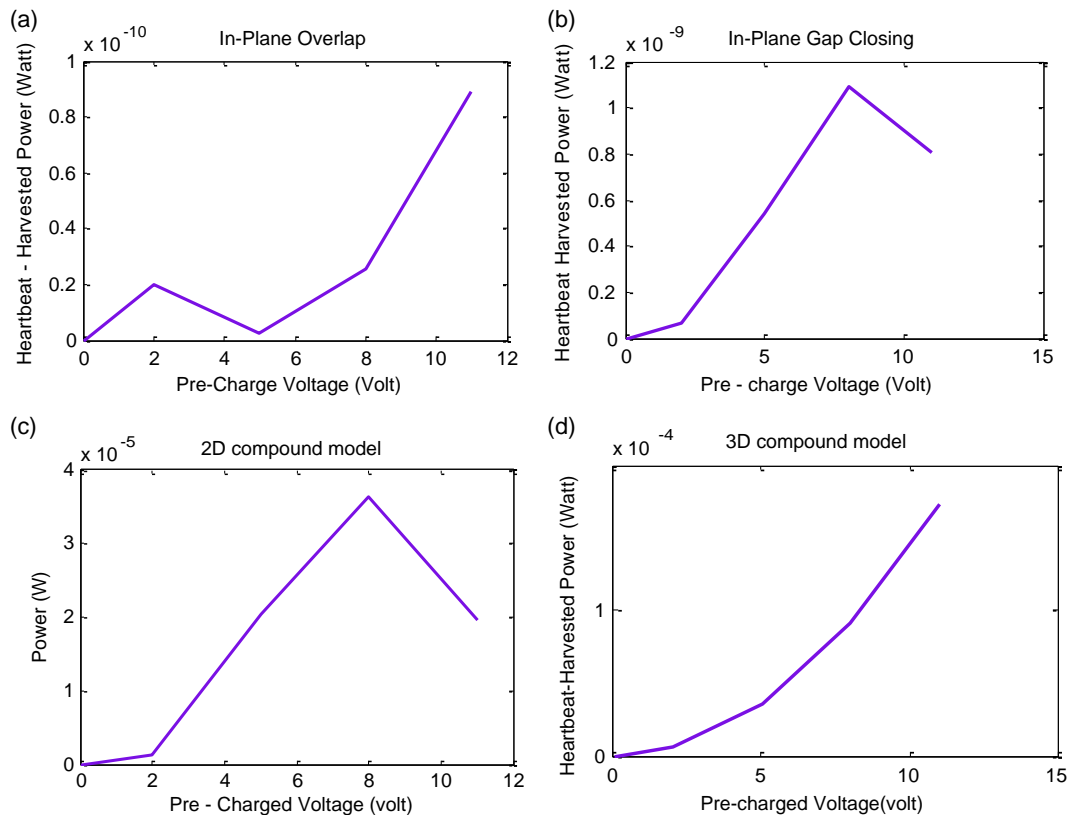


Figure 22. Power versus pre-charge voltage of different harvesters for: a) In-plane overlap, b) in-plane gap closing, c) 2D compound, and d) 3D compound models.

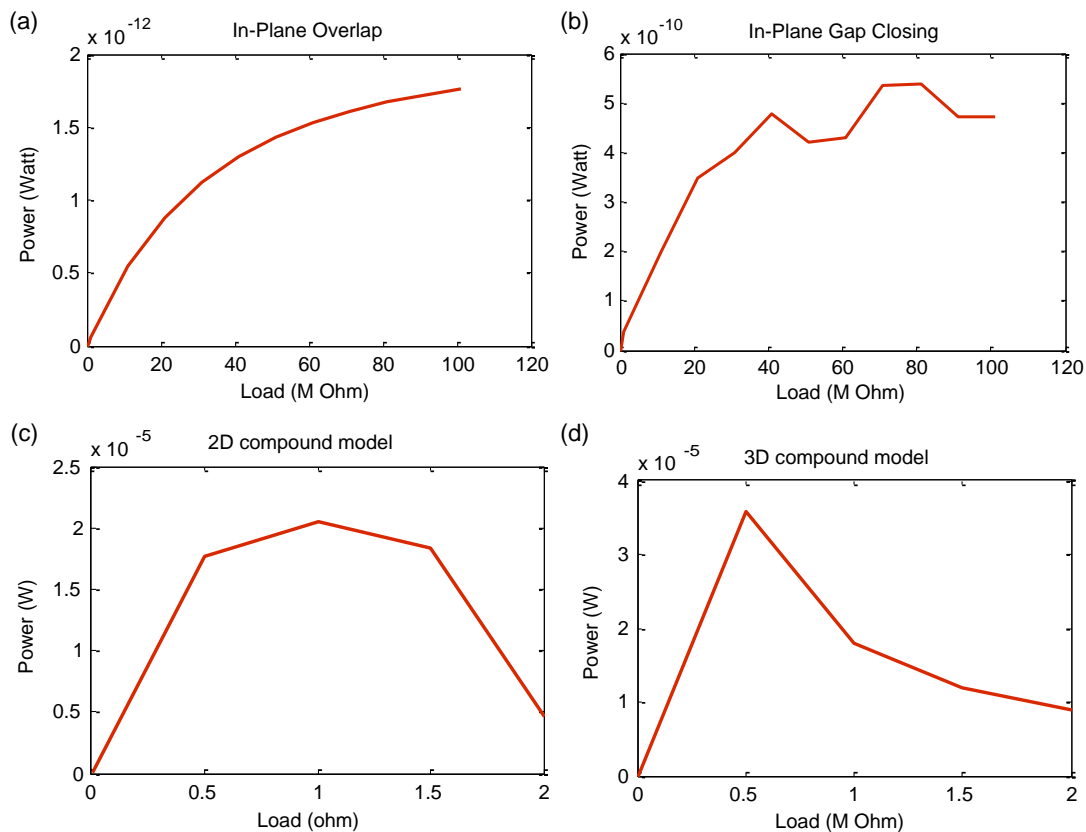


Figure 23. Sensitivity of different heartbeat energy harvesters to loading impedance for: a) In-plane overlap, b) in-plane gap closing, c) 2D compound, and d) 3D compound models.

10. Conclusion

To simulate the performance of different electrostatic energy harvesters under heartbeat excitation, comprehensive models of 1D, 2D, and 3D electrostatic energy harvesters were developed in state-space equation forms. For optimal harvesting, the recorded acceleration of heartbeats in interventricular septum was introduced as the system input. In this case, the 1D structure was optimally designed to be implemented in $5000 \times 5000 \times 100$ (μm)³ while the others were the development of the 1D model with the same volume. Simulation results showed that under the same excitation, multidimensional models can potentially gain much higher energy than 1D models. Evaluation of the harvesters under different loading conditions also revealed that the maximum energy of all ($35.08 \mu\text{W}$) was harvested by the 3D model at loading around $0.5 \text{ M}\Omega$ under a specific exposure to the heartbeat excitation vector. This amount of power can satisfactorily serve the majority of the energy needs of pacemakers and even more optimization of the model can eliminate the need for their battery.

Conflict of Interest

The authors declare no conflict of interest.

Data Availability Statement

Research data are not shared.

Keywords

compound structures, electrostatic energy, heartbeat energy harvesting, in-plane gap closing, in-plane gap overlap, MEMS

Received: May 26, 2023

Revised: July 15, 2023

Published online: September 5, 2023

- [1] P. Mitcheson, E. Yeatman, G. Rao, A. Holmes, T. Green, *Proc. IEEE* **2008**, *96*, 1457.
- [2] A. Harb, *Renewable Energy* **2011**, *36*, 2641.
- [3] P. D. Mitcheson, T. C. Green, *IEEE Trans. Circuits Syst.* **2012**, *59*, 3098.
- [4] E. Blokhina, D. Galayko, P. Basset, O. Feely, *IEEE Trans. Circuits Syst. I* **2013**, *60*, 875.
- [5] E. Blokhina, D. Galayko, P. Harte, P. Basset, O. Feely, *Appl. Phys. Lett.* **2012**, *101*, 173904.
- [6] M. Deterre, B. Boutaud, R. Dalmolin, S. Boisseau, J. Chaillout, E. Lefeuvre, E. Dufour-Gergam, *Energy Harvesting System For Cardiac Implant Applications*, DTIP of MEMS and MOEMS, France, **2011**.
- [7] J. Lueke, W. A. Moussa, *Sensors* **2011**, *11*, 1433.

- [8] M. A. Karami, D. J. Inman, *Appl. Phys. Lett.* **2012**, *100*, 042901.
- [9] S. Roundy, P. K. Wright, K. S. Pister, in *Proc. 2002 ASME Int. Mechanical Engineering Congress and Exposition*, New Orleans, LA, November 2002.
- [10] R. Guillemet, P. Basset, D. Galayko, T. Bourouina, *Procedia Eng.* **2010**, *5*, 1172.
- [11] S. Meninger, J. O. Mur-Miranda, R. Amirtharajah, A. P. Chandrakasan, J. H. Lang, *IEEE Trans. Very Large Scale (VLSI) Syst.* **2001**, *9*, 64.
- [12] G. Despesse, T. Jager, J. J. Chaillout, J. M. Lger, A. Vassilev, S. Basrour, B. Charlot, in *Proc. of DTIP of MEMS & MOEMS conference*, Switzerland, June 2005.
- [13] Y. Zhu, S. O. R. Moheimani, M. R. Yuce, *IEEE Sensors Conf.*, IEEE, Piscataway, NJ October 2009, pp. 1542–1545.
- [14] A. G. Fowler, S. O. R. Moheimani, S. Behrens, *IEEE Sensors Conf.*, IEEE, Taipei October 2012, pp. 1–4.
- [15] Z. Li, Y. Liu, P. Yin, Y. Peng, J. Luo, S. Xie, H. Pu, *Int. J. Mech. Sci.* **2021**, *198*, 1.
- [16] Y. Peng, W. Xu, Y. Gong, X. Jiang, Z. Li, *J. Phys.: Conf. Ser.* **2023**, *2477*, 1.
- [17] Z. Li, Z. Yan, J. Luo, Z. Yang, *Energy Convers. Manage.* **2019**, *179*, 132.
- [18] L. G. W. Tvedt, L.-C. J. Blystad, E. Halvorsen, *DTIP of MEMS and MOEMS Conf.*, Norway, April 2008.
- [19] B. D. Truong, C. P. Le, *Int. J. Circuit Theory Appl.* **2023**, *51*, 2518.
- [20] VS Mallela, V Ilankumaran, NS. Rao, *Indian Pacing Electrophysiol. J.* **2004**, *4*, 201.